Acta Cryst. (1988). B44, 263–271

Tetramethylammonium Hexacyanotrimethylenecyclopropanide: Crystal Structure of Antiferromagnetic Phase II and Paramagnetic Phase I

BY S. C. ABRAHAMS AND P. MARSH

AT&T Bell Laboratories, Murray Hill, New Jersey 07974, *USA*

AND L. A. DEURING*

Chemistry Department, Columbia University, New York, NY 10027, *USA*

(*Received* 8 *October* 1987; *accepted* 17 *December* 1987)

Abstract

$C_4H_{12}N^+.C_{12}N_6^-$ undergoes a transition at 364 K from triclinic phase II to monoclinic phase I as the temperature increases. $M_r = 302{\cdot}32$. Phase II, $P\bar{1}$ with $a = 11{\cdot}473\ (3)$, $b = 12{\cdot}002\ (3)$, $c = 6{\cdot}811\ (2)$ Å, $\alpha = 104{\cdot}55\ (2)$, $\beta = 101{\cdot}40\ (2)$, $\gamma = 67{\cdot}85\ (2)°$, $V = 835{\cdot}1\ (7)$ Å^3, $Z = 2$, $D_m = 1{\cdot}19\ (2)$, $D_x = 1{\cdot}202$ Mg m^{-3}, λ(Mo $K\alpha$) = 0·71073 Å, $\mu = 7{\cdot}35$ mm^{-1}, $F(000) = 314$ e, $T = 294$ K, $wR_{int} = 0{\cdot}0137$ for 4897 F_m, with final $wR = 0{\cdot}0218$ for 2140 independent averaged $F_m^2 \geq 2\sigma(F_m^2)$. Phase I, $C2/m$ with $a = 19{\cdot}760\ (13)$, $b = 13{\cdot}195\ (7)$, $c = 6{\cdot}913\ (6)$ Å, $\beta = 106{\cdot}63\ (6)°$, $V = 1727{\cdot}1\ (36)$ Å^3, $Z = 4$, $D_x = 1{\cdot}163$ Mg m^{-3}, λ(Mo $K\alpha$) = 0·71073 Å, $\mu = 7{\cdot}11$ mm^{-1}, $F(000) = 628$ e, $T = 388$ K, $wR_{int} = 0{\cdot}0234$ for 2614 F_m, with final $wR = 0{\cdot}0317$ for 599 independent averaged $F_m^2 \geq 2\sigma(F_m^2)$. The hexacyanocyclopropanide anion at 294 K is planar, within ±0·024 Å, and is close to $3m$ symmetry. The C–C bond distance in the cyclopropanide ring is 1·402 (3) Å, with C_{ring}–$C_{methylene} = 1{\cdot}367\ (2)$, $C_{methylene}$–$C_{cyano} = 1{\cdot}418\ (5)$ and C–N = 1·145 (3) Å. In the cation, N–CH_3 = 1·418 (32) Å for phase II. Corresponding distances for phase I are 1·391 (5), 1·363 (17), 1·414 (8), 1·139 (6) and 1·286 (72) Å respectively. Short N···N contacts of 3·189 (3) and 3·256 (3) Å, inclined respectively at 4·4 (1) and 0·4 (1)° to the anion plane, form between radical anions. The radicals also form stacks, normal to the anion plane, with π-electron overlap between alternating pairs resulting in separations of only 3·24 Å; these pairs are connected by normal stack distances of 3·44 Å. Together, the near-planar and in-stack contacts result in puckered sheets of strongly linked radical anions in phase II. Magnetic exchange interactions between the radical anions give quasi-two-dimensional antiferromagnetic spin coupling at low temperatures. Above the transition temperature, the in-stack coupling decreases as the π-electron overlap contacts increase in length by about 0·1 Å. The short N···N contacts close to the molecular plane remain unchanged in phase I, resulting in a quasi-one-dimensional array. As the magnetic order along the column direction decreases, the remaining exchange interactions result in the paramagnetism of phase I.

Introduction

A magnetic and structural phase transition at 363·7 K has been found in $[(CH_3)_4N]^+.[C_3\{C(CN)_2\}_3]^-$ (hereafter HCTMCP$^-$ for the anion), a material first synthesized as an intermediate in the search for a purely organic ferromagnet (Abrahams, Bair, DiSalvo, Marsh & Deuring, 1984). The magnetic susceptibility temperature dependence is indicative of a strong magnetic coupling between spins associated with the HCTMCP$^-$ radical anion [see (I)].

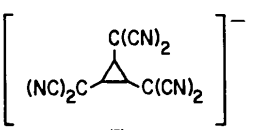

(I)

The coupling was postulated to be primarily antiferromagnetic below and paramagnetic above the phase transition, which was found to be reversible with an identical lambda-type specific-heat anomaly observed on both heating and cooling. The triclinic symmetry below 363·7 K transforms to monoclinic symmetry above as the unit-cell volume exactly doubles, within experimental error. Unlike the recently synthesized organic salts of tetramethyltetraselenafulvalene $[(TMTSF)_2X]$, $X = AsF_6^-$, PF_6^-, ClO_4^-, ReO_4^- (Mortensen, 1982; Pouget, Shirane, Bechgaard & Fabre, 1983; Rindorf, Soling & Thorup, 1982), which develop antiferromagnetism below 10 K and become superconducting near 1 K, $[(CH_3)_4N]^+$.HCTMCP$^-$ is highly resistive, indicating the spins to be localized on each molecule.

* Present address: Mail Stop D 317, Varian Associates, 611 Hansen Way, Palo Alto, CA 94303, USA.

0108-7681/88/030263-09$03.00

© 1988 International Union of Crystallography

The structural changes from low-temperature phase II to high-temperature phase I in $[(CH_3)_4N]^+.HCTMCP^-$ and the resulting relationships to the magnetic properties in the two phases, also referred to throughout this paper as antiferromagnetic and paramagnetic respectively, are presented hereunder together with the structure of both phases.

Experimental

The synthesis of $[(CH_3)_4N]^+.HCTMCP^-$, the growth and habit of the very deep reddish-purple crystals, and the results of chemical analysis have been given by Abrahams *et al.* (1984), together with the lattice-parameter variation in the temperature range 294 to 407 K. The Laue symmetry of phase II is $\bar{1}$, that of phase I is $2/m$. Crystal data for phase II at 294 K and for phase I at 388 K are given in the *Abstract*. There are no systematic absences in phase II: the only absences for phase I are in hkl for $h + k = 2n + 1$. The monoclinic unit cell of phase I is related to the triclinic cell of phase II by the matrix transformation $110/\bar{1}10/001$.

Integrated intensity measurements for phase II were made on a crystal with dimensions $0{\cdot}146 \times 0{\cdot}123 \times 0{\cdot}112$ mm bounded by {001}, {010} and {100} and mounted on a Pyrex capillary in an Enraf–Nonius CAD-4 diffractometer controlled by a PDP11/24-8e minicomputer under Enraf–Nonius (1982) software. Radiation was Mo $K\alpha$ from a graphite monochromator with ω–2θ scan range of $0{\cdot}85° + 0{\cdot}35°\tan\theta$. Backgrounds were estimated by extending the scan 25% on either side of the peak, with maximum time of 240 s per reflection. All reflections with $-16 \le h \le 16$, $-16 \le k \le 16$, $-10 \le l \le 10$ and $(\sin\theta)/\lambda \le 0{\cdot}7035$ Å^{-1} were measured. Six standard reflections were measured every 6 h. Variations among the standards ranged from 1·2 to 2·4%. A linear isotropic decline in the integrated intensities was determined by the method of Abrahams & Marsh (1987), with $I_t = I_0[1-0{\cdot}000058(2)t]$ where I_t is the integrated intensity at th and I_0 is the corresponding value at zero exposure. The maximum decline due to radiation damage is hence about 2·51% over the 433 h of measurement. D_m determined pycnometrically. 12003 reflections were measured, of which 4897 were greater than 2 e.s.d. based only on counting statistics. Following correction for Lorentz, polarization, absorption (transmission factors were in the range 98·83 to 98·84%) and radiation-damage effects, the resulting 2151 $F_m^2 \ge 2\sigma F_m^2$ averaged Friedel pairs had $R_{int} = 0{\cdot}0165$, $wR_{int} = 0{\cdot}0137$ excluding 11 outlier pairs, and gave a moderately linear δm normal probability plot (Abrahams & Keve, 1971) with $\mathcal{S}(\delta m) = 0{\cdot}65$ and zero intercept.

Crystal dimensions for phase I intensity measurements were $0{\cdot}103 \times 0{\cdot}093 \times 0{\cdot}091$ mm, corresponding to a morphology bounded by {001}, {110} and {$\bar{1}$10}. This crystal was mounted in a microfurnace (Lissalde, Abrahams & Bernstein, 1978) on the CAD-4 diffractometer, operated as for phase II and with a temperature stability of $\pm 0{\cdot}25$ K. All reflections with $-19 \le h \le 19$, $-13 \le k \le 13$, $-6 \le l \le 6$ and $(\sin\theta)/\lambda \le 0{\cdot}4812$ Å^{-1} were measured. The six standards suffered a linear decrease with exposure: the total isotropic decline, determined as for phase II on all reflections measured, is given by $I_t = I_0[1-0{\cdot}00032(1)t]$, for t in hours. The maximum exposure was 236 h, for a maximum correction of about 5·2%. 3902 reflections were measured at 388 K, with 2614 greater than 2 e.s.d. (counting statistics), giving 616 symmetry-independent $F_m^2 \ge 2\sigma F_m^2$: excluding 17 outliers, $R_{int} = 0{\cdot}0292$, $wR_{int} = 0{\cdot}0234$. The δm plot was rather more linear than was that at 294 K, with $\mathcal{S}(\delta m) = 0{\cdot}95$ and intercept of nearly zero.

Standard deviations (σF_m) in the averaged independent structure factors were derived by a variation of Abrahams, Bernstein & Keve's (1971) method in which $\sigma^2 F_m^2$ is taken as the greater of V_1 or V_2, where V_1 is the internal variance calculated from differences among the members of a form (two in phase II, four in phase I) and V_2 is the sum of the variances due to counting statistics, absorption and replication variations in the standards. $wF_m^2 = 1/\sigma^2(F_m^2)$.

Structure determination and refinement

Repeated attempts to solve the structure of phase II by symbolic addition, using *MULTAN*78 (Main, Hull, Lessinger, Germain, Declercq & Woolfson, 1978), were unsuccessful. The relatively short c axis and location of inversion centers in the unit cell together with the expected shape of the $HCTMCP^-$ radical anion favored the possibility that the latter would not be far from positions midway between inversion centers with the anion plane oriented approximately normal to **c**. An idealized version of the $HCTMCP^-$ radical anion was hence placed at each such location and its orientation and position refined by the method of least squares, in which rotation and translation only of the rigid group was permitted. A minimum in R (at 0·27) was found only for the anion center located at 0, 0, $\frac{1}{4}$ and $\frac{1}{2}$, 0, $\frac{3}{4}$: all other locations gave $R > 0{\cdot}5$. A difference Fourier series based on the refined model gave the C- and N-atom positions of the $[(CH_3)_4N]^+$ cation. Calculations were initially made on the PDP11/24 minicomputer with the *ORFLS*-4 (Busing, Martin & Levy, 1973) and *FORDUP* Fourier series (Lundgren, 1982) programs and subsequently on our VAX11/750 superminicomputer with a locally modified and expanded version of *ORFLS*-4 and a locally written Fourier-series program, using atomic scattering factors from *International Tables for X-ray Crystallography* (1974).

The locations of the methyl-group H atoms were not apparent in subsequent difference Fourier series, hence

Table 1. *Atomic positional parameters and equivalent isotropic thermal parameters* (Å)

U_{eq} is the r.m.s. radial displacement amplitude.

	x	y	z	U_{eq}
Phase II (294 K)				
C(1)	0·4971 (1)	0·0243 (1)	0·7524 (2)	0·21 (3)
C(2)	0·6173 (1)	0·0289 (1)	0·8365 (2)	0·21 (3)
C(3)	0·5132 (1)	0·1380 (1)	0·8288 (2)	0·21 (2)
C(4)	0·4188 (1)	−0·0415 (1)	0·6631 (2)	0·22 (2)
C(5)	0·7433 (1)	−0·0265 (1)	0·8929 (2)	0·23 (2)
C(6)	0·4663 (1)	0·2631 (1)	0·8698 (2)	0·23 (1)
C(7)	0·2879 (2)	0·0176 (1)	0·6116 (2)	0·23 (2)
C(8)	0·4658 (1)	−0·1714 (1)	0·6241 (2)	0·23 (2)
C(9)	0·7990 (1)	−0·1567 (2)	0·8596 (2)	0·25 (3)
C(10)	0·8184 (1)	0·0467 (2)	0·9866 (2)	0·25 (4)
C(11)	0·5496 (2)	0·3292 (1)	0·9635 (2)	0·25 (3)
C(12)	0·3360 (2)	0·3283 (1)	0·8164 (2)	0·24 (2)
N(1)	0·1820 (1)	0·0654 (1)	0·5680 (2)	0·29 (4)
N(2)	0·5035 (1)	−0·2767 (1)	0·5896 (2)	0·28 (4)
N(3)	0·8414 (1)	−0·2616 (1)	0·8323 (2)	0·30 (5)
N(4)	0·8742 (1)	0·1109 (2)	1·0617 (3)	0·31 (7)
N(5)	0·6205 (2)	0·3777 (1)	1·0380 (3)	0·30 (7)
N(6)	0·2311 (1)	0·3788 (1)	0·7731 (2)	0·29 (5)
N(1*c*)	0·8486 (6)	0·3615 (5)	0·6206 (7)	0·23 (2)
C(1*c*)	0·9200 (7)	0·3624 (7)	0·4663 (11)	0·39 (7)
C(2*c*)	0·8508 (8)	0·2424 (8)	0·6118 (15)	0·42 (9)
C(3*c*)	0·7202 (6)	0·4408 (7)	0·5981 (11)	0·40 (11)
C(4*c*)	0·9061 (9)	0·4022 (10)	0·8090 (14)	0·45 (14)
Phase I (388 K)				
C(1)	0·5118 (2)	0	0·7578 (5)	0·27 (4)
C(2)	0·5748 (1)	0·0527 (2)	0·8348 (3)	0·28 (3)
C(4)	0·4396 (2)	0	0·6689 (5)	0·29 (4)
C(5)	0·6113 (2)	0·1413 (2)	0·8801 (4)	0·30 (1)
C(8)	0·4016 (2)	0·0918 (3)	0·6240 (5)	0·32 (5)
C(9)	0·5777 (2)	0·2362 (3)	0·8393 (5)	0·33 (2)
C(10)	0·6855 (2)	0·1373 (2)	0·9710 (5)	0·33 (4)
N(2)	0·3699 (2)	0·1644 (3)	0·5858 (6)	0·38 (7)
N(3)	0·5495 (2)	0·3127 (3)	0·8047 (5)	0·38 (7)
N(4)	0·7448 (2)	0·1303 (2)	1·0437 (6)	0·39 (9)
N(1*c*)	0·8595 (8)	0	0·624 (3)	0·29 (3)
C(1*c*)	0·8910 (18)	0	0·496 (4)	0·56 (15)
C(2*c*)	0·8147 (7)	0·0793 (11)	0·593 (3)	0·57 (18)
C(4*c*)	0·8999 (17)	0	0·796 (3)	0·56 (16)

they were placed at three corners of a regular tetrahedron with the methyl C atom at the fourth and assumed initially to rotate freely about the tetrahedron axis, with scattering given by a Bessel function. The C–H distance was taken as 0·95 Å and the H–C–H and H–C–N angles as 109·47°. The fit improved on modifying the model to allow for hindered rotation by these H atoms, and further improved slightly (significantly, at the 0·005 confidence level) for partially hindered rotation. Final atomic coordinates, based on anisotropic thermal parameters for all anion atoms but allowing the cation N atom and CH_3 groups to undergo anharmonic vibration to fourth order, with correction for anisotropic extinction based upon Becker & Coppens' (1975) formalism, are given in Table 1.* The extinction correction corresponded to a mosaic anisotropy with Z_{ii} ranging from 22·8 (4) to 19·7 (6) μm: improved robustness in least-squares refinement resulted on varying the squared rather than the usual extinction-parameter function. A significant decrease in wR (~4·5%) accompanied the change from isotropic to anisotropic extinction. The maximum resulting extinction correction was 33·0%, in $F(221)$. The residual electron density in the anion plane as given by the difference Fourier series at this stage suggested the presence of a small anionic disorder component that was rotated about 60° from the principal component. Refinement showed that the disorder component was about 1·09 (10)% of the complete anion: the resulting improvement in wR (~0·7%) was sufficient not to reject the disorder hypothesis at the 0·005 significance level. It may be noted that the refined center position of the $HCTMCP^-$ radical anion is located only about 1 Å from the position assumed for the model, also that the normal to the anion plane is inclined at 11·8° to **c**, in contrast to the assumed parallel orientation. The anion atom labelling is given in Fig. 1.

Location of the anion in phase I was deduced from that in phase II by assuming the minimum atomic displacements for coincidence between the mirror planes in $C2/m$ and that normal to the $HCTMCP^-$ anion. Refinement thereafter followed as for phase II. A correction for anisotropic rather than isotropic extinction was again found necessary, with final Z_{ii} ranging from 25 (1) to 14 (3) μm. The maximum extinction correction for phase I was 33·7% in $F(\bar{2}02)$. The largest ratio of shift to e.s.d. in C or N atomic coordinate was 0·39 for N(5) in phase II and 0·01 in phase I for the final refinement cycle. Final refinement indicators (on F) are $R = 0{\cdot}0334$, $wR = 0{\cdot}0218$, $S = 1{\cdot}518$ for phase II based on 2140 reflections with $F_m^2 \geq 2\sigma F_m^2$ and $R = 0{\cdot}0331$, $wR = 0{\cdot}0317$, $S = 1{\cdot}779$ for phase I based on 599 reflections with $F_m^2 \geq 2\sigma F_m^2$. Both δR plots corresponding to the final models for phases I and II were rather linear with zero intercepts and nearly

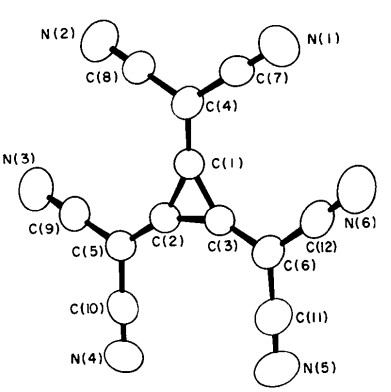

Fig. 1. $[(CH_3)_4N]^+.HCTMCP^-$. Atomic labelling and thermal ellipsoids at 50% probability for the radical anion at 294 K (Johnson, 1976).

* Lists of structure factors, anisotropic thermal parameters with anharmonic tensor coefficients and anisotropic extinction coefficients for phases I and II have been deposited with the British Library Document Supply Centre as Supplementary Publication No. SUP 44638 (37 pp.). Copies may be obtained through The Executive Secretary, International Union of Crystallography, 5 Abbey Square, Chester CH1 2HU, England.

Table 2. *Intraionic bond lengths* (Å) *and angles* (°) *in* $(CH_3)_4N^+.HCTMCP^-$

	294 K Phase II	388 K Phase I
C(1)–C(2)	1·400 (2)	1·391 (5)
C(2)–C(3)	1·405 (2)	1·391 (6)
C(3)–C(1)	1·400 (2)	
C(1)–C(4)	1·370 (2)	1·383 (6)
C(2)–C(5)	1·366 (2)	1·353 (5)
C(3)–C(6)	1·365 (2)	
C(4)–C(7)	1·412 (2)	
C(4)–C(8)	1·416 (2)	1·412 (4)
C(5)–C(9)	1·423 (2)	1·407 (5)
C(5)–C(10)	1·412 (3)	1·422 (5)
C(6)–C(11)	1·422 (2)	
C(6)–C(12)	1·423 (2)	
C(7)–N(1)	1·146 (2)	
C(8)–N(2)	1·149 (2)	1·133 (5)
C(9)–N(3)	1·146 (2)	1·145 (5)
C(10)–N(4)	1·144 (3)	1·139 (5)
C(11)–N(5)	1·142 (3)	
C(12)–N(6)	1·141 (2)	
N(1*c*)–C(1*c*)	1·459 (11)	1·216 (41)
N(1*c*)–C(2*c*)	1·406 (12)	1·348 (17)
N(1*c*)–C(3*c*)	1·424 (8)	
N(1*c*)–C(4*c*)	1·383 (10)	1·230 (24)
C(1)–C(2)–C(3)	59·9 (1)	60·0 (2)
C(2)–C(3)–C(1)	59·9 (1)	60·0 (2)
C(3)–C(1)–C(2)	60·2 (1)	60·0 (2)
C(2)–C(1)–C(4)	150·5 (1)	150·0 (2)
C(3)–C(1)–C(4)	149·3 (1)	150·0 (2)
C(1)–C(2)–C(5)	151·7 (1)	150·9 (3)
C(3)–C(2)–C(5)	148·4 (1)	149·1 (2)
C(1)–C(3)–C(6)	151·3 (1)	150·9 (3)
C(2)–C(3)–C(6)	148·8 (1)	149·1 (2)

identical slopes. The largest features in the final difference Fourier series are ± 0.11 e Å^{-3} for phase II, ± 0.10 e Å^{-3} for phase I. The arrangement of cations and radical anions in both phases is shown in Fig. 2.

Amplitudes of vibration

The r.m.s. radial amplitude of thermal vibration $\bar{u}$ for each atom in both phases is given in Table 1. The amplitude of all anion C atoms is rather constant in phase II with an average of 0·23 (2) Å, the terminal cyano N atoms having a larger but also constant average amplitude of 0·30 (1) Å. These radial amplitudes increase significantly in phase I at 388 K to 0·31 (2) Å for the anion C atoms and 0·38 (1) Å for the cyano N atoms. A larger increase in the average cation methyl-C-atom amplitude occurs, from 0·42 (2) Å in phase II to 0·57 (1) Å in phase I. All atoms in the anion undergo anisotropic displacements, with the largest anisotropy exhibited by the cyano N atoms: *e.g.* N(4) has $u_{33} = 0.38$, $u_{11} = 0.25$ Å at 294 K and 0·49, 0·31 Å at 388 K. Greater anisotropy is found on the cation C atoms, with C(4*c*) having $u_{33} = 0.57$, $u_{11} = 0.30$ Å at 294 K and 0·74, 0·38 Å at 388 K. Highly significant improvement in the value of wR is obtained by substituting anisotropic for isotropic thermal parameters in the refinement model, and further improvement is gained on adding anharmonic coefficients to fourth order in phase II and third order in phase I.

Intraionic connective geometry

The bond lengths in both phases of the $HCTMCP^-$ radical anion, given in Table 2, are of intrinsic interest since the present study provides one of the first measurements of the trimethylenecyclopropanide ion dimensions. The comprehensive survey of nearly 300 cyclopropane derivatives by Allen (1980) contained only one example of a trimethylenic substituted cyclopropane, triisopropylidenecyclopropane (Dietrich, 1970), in which the average C_{ring}–C_{ring} distance is 1·451 (11), C=C is 1·333 (1) and C–C_{methyl} is 1·496 (11) Å. The C_{ring}–C_{ring} distance in phase II of 1·402 (3) Å {the e.s.d. of the average $\bar{x} = 1/n \sum_{i=1}^{n} x_i$ is taken as $[1/(n-1) \sum_{i=1}^{n} (x_i - \bar{x})^2]^{1/2}$} is very significantly shorter than that in triisopropylidenecyclopropane, which provided the shortest distance found in Allen's (1980) survey. By contrast, the mean C_{ring}–C_{ring} distance in cyclopropane with only C(sp^3) or H as substituents is given by Allen (1980) as 1·508 (3) Å. A very recent report by Ward (1987) on donor–acceptor complexes with $HCTMCP^{n-}$ as anion gives an average C_{ring}–C_{ring} distance of 1·387 (8) Å in five complexes for which $n = 1$ or 2, in good agreement with our present results. Introduction of the unpaired electron associated with the radical ion into the cyclopropane ring is expected to result in a shorter C–C distance, owing to the contribution of components such as those shown in Fig. 3 to the ground state of $HCTMCP^-$.

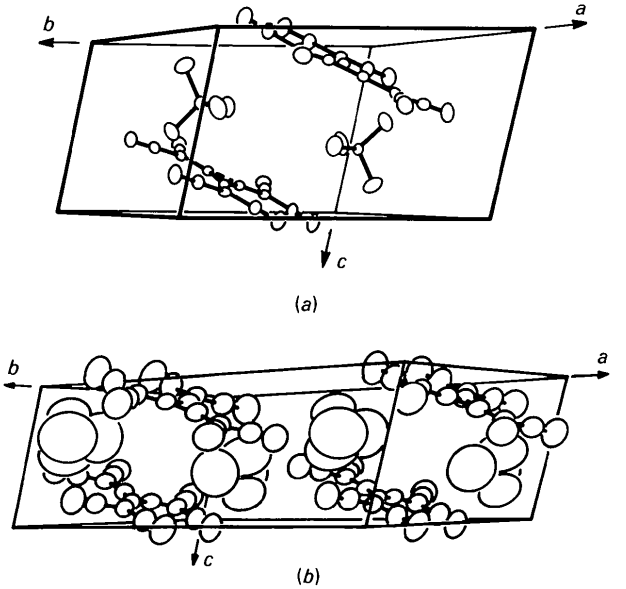

Fig. 2. (*a*) Content of unit cell for phase II at 294 K. (*b*) Content of unit cell for phase I at 388 K, with molecular orientation comparable to that in (*a*).

The cyclopropanide-ring distance of 1·402 (3) Å in phase II may also be compared with the corresponding ring distance of 1·373 (5) Å reported in *sym*-triphenylcyclopropenium perchlorate by Sundaralingam & Jensen (1966), since the bonding character of both anion and cation rings may be represented as fully delocalized. The cyclopropanide-ring distance may further be compared with the localized C–C distance of 1·416 (7) Å and C=C distance of 1·341 (8) Å in di-*p*-tolylbis(trifluoromethyl)triafulvene (Ammon, Sherrer & Agranat, 1977): the average 1·391 (8) Å in the latter three-membered ring is not significantly different from either our present value or that of Ward (1987). The C_{ring}–$C_{methylene}$ distance in phase II of 1·367 (2) Å is closer to that of a double bond [Sutton (1965) gives C=C = 1·335 Å], as expected from Fig. 3, than the 1·387 (11) Å distance reported by Ward (1987). The C≡N bond length of 1·145 (3) Å in phase II does not differ significantly from the 1·130 (24) Å found by Ward (1987), the 1·151 (4) Å C≡N distance reported in the tetracyanoquinodimethane (TCNQ) radical anion by Kistenmacher, Phillips & Cowan (1974) or the 1·141 (5) Å distance in the same anion of a different salt studied by Jaud, Chasseau, Gaultier & Hauw (1974). The nominally single $C_{methylene}$–C_{cyano} bond of length 1·418 (5) Å is not significantly different from that reported by Ward (1987) for $HCTMCP^{n-}$ of 1·420 (1) Å. The $HCTMCP^-$ radical ion in phase II is close to planar, with no deviation from the mean plane greater than 0·024 (1) Å [by N(2) and N(3)]. The equation of the least-squares fit to the mean anion plane, in triclinic crystal coordinates, is $-0{\cdot}01834(2)X+0{\cdot}00026(1)Y+0{\cdot}13371(1)Z-0{\cdot}009954(3)=0$. Average distances within the anion of phase I at 388 K, see Table 2, are not significantly different from those in phase II at 294 K although all are systematically smaller due to the increased amplitudes of thermal motion, see above.

The tetramethylammonium ion geometry in phase II appears normal, for all atoms assumed to undergo harmonic thermal vibrations, with C–N = 1·488 (18) Å and C–N–C = 109·5 (1·6)°: however, the addition of anharmonic terms gives the bond lengths in Table 2, with average C–N = 1·418 (32) Å and C–N–C angle of 109·5 (1·7)°. The foreshortening of the C–N distance at 294 K is hence a function of the thermal-motion description that becomes more pronounced at 388 K. At this temperature, the C–N distance has an average value of only 1·286 (72) Å. The standard C–N length is 1·479 (5) Å (Sutton, 1965), with regular tetrahedral angle of 109·5°.

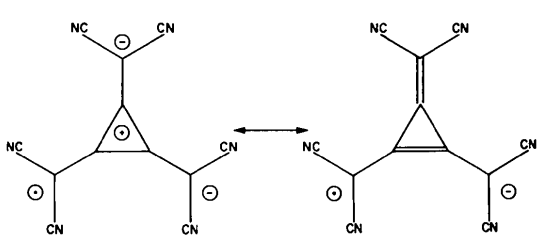

Fig. 3. Contributions to ground state of $HCTMCP^-$ radical anion.

Structural rearrangement at the phase transition

The atomic coordinates determined for phase II at 294 K, see Table 1, may be transformed to have an orientation comparable with those in the phase I monoclinic unit cell as given in Table 3. A pseudo-mirror plane relationship is thereby revealed in which some atoms have y' coordinates close to zero and other atoms form related pairs with $x'_1 \simeq x'_2$, $y'_1 \simeq -y'_2$, $z'_1 \simeq z'_2$. A new set of coordinates $x''y''z''$ can thereupon be derived in which the incipient mirror plane at $y''=0$ becomes fully operational. These coordinates may be regarded as precursors to those determined in phase I at 388 K, although the crystal symmetry at 294 K is triclinic and hence the $x''y''z''$ set does not in fact exist. Nevertheless, it is of interest to note that the displacements required at 294 K in order to impose mirror symmetry on the triclinic atomic coordinates range from 0·12 to 0·37 Å for the anion and from 0·03 to 0·51 Å for the cation (see Δ in Table 3).

The atomic displacements necessary to transform the structure at 294 K into that at 388 K may be obtained directly from the differences between the $x'y'z'$ set of Table 3 and the experimental set for phase I in Table 1, assuming identical lattice constants for both sets. These displacements, which range from 0·12 to 0·35 Å for the anion and 0·11 to 0·53 Å for the cation, are closely comparable to the displacements between $x'y'z'$ and $x''y''z''$ in Table 3. Displacements between the precursor coordinates $x''y''z''$ at 294 K and those in phase I at 388 K are considerably smaller, ranging from 0·02 to 0·05 Å for the anion and 0·08 to 0·21 Å for the cation. It may hence be inferred that the major rotations in the $[(CH_3)_4N]^+$ and $(HCTMCP)^-$ ions occur as the crystallographic mirror plane develops, with much smaller rotations ensuing at higher temperatures. Such a model is also consistent with the lattice-constant temperature dependence, see Abrahams *et al.* (1984). The total rotation by the cation between 298 and 388 K is about 16·5° as the anion rotates about 5° in its own plane and a further 3° out of plane.

$HCTMCP^-$ radical anion array at 294 K

The combination of symmetry operators and number of $HCTMCP^-$ radical anions in the triclinic and monoclinic unit cells requires that all anions in either phase be parallel. The arrangement of anions in phase II is characterized by two sets of close contacts: one set of interactions is oriented close to the anion plane, the other is nearly normal to the plane. The arrangement of

Table 3. *Transformed phase* II *coordinates at* 294 K, *corresponding set with mirror symmetry, and displacement between sets*

$x' = (x + y + \frac{1}{2})/2$, $y' = (x - y - \frac{1}{2})/2$, $z' = z$, see Table 1 for xyz coordinates in phase II. Atoms with $y' \simeq 0$ have $y'' = 0$. Pairs of atoms 1 and 2 with $x'_1 \simeq x'_2$, $y'_1 \simeq -y'_2$, $z'_1 \simeq z'_2$ have $x'' = (x'_1 + x'_2)/2$, $y'' = \pm(y'_1 - y'_2)/2$, $z'' = (z'_1 + z'_2)/2$. Δ is the displacement between an atom at $x'y'z'$ and $x''y''z''$, based on the transformed unit cell with $a' = 19{\cdot}481$, $b' = 13{\cdot}109$, $c' = 6{\cdot}811$ Å, $\alpha' = 93{\cdot}27$, $\beta' = 105{\cdot}74$ and $\gamma' = 92{\cdot}78°$ obtained by $\mathbf{a}' = \mathbf{a} + \mathbf{b}$, $\mathbf{b}' = -\mathbf{a} + \mathbf{b}$, $\mathbf{c}' = \mathbf{c}$.

	x'	y'	z'	x''	y''	z''	Δ(Å)
C(1)	0·5107	−0·0136	0·7524	0·5107	0	0·7524	0·178 (4)
C(2)	0·5731	0·0442	0·8365	0·5744	0·0533	0·8327	0·126 (4)
C(3)	0·5756	−0·0624	0·8288	0·5744	−0·0533	0·8327	0·126 (4)
C(4)	0·4387	−0·0199	0·6631	0·4387	0	0·6631	0·260 (4)
C(5)	0·6084	0·1349	0·8929	0·6116	0·1417	0·8814	0·143 (4)
C(6)	0·6147	−0·1484	0·8698	0·6116	−0·1417	0·8814	0·143 (4)
C(7)	0·4028	−0·1149	0·6116	0·3999	−0·0917	0·6178	0·313 (4)
C(8)	0·3972	0·0686	0·6241	0·3999	0·0917	0·6178	0·313 (4)
C(9)	0·5712	0·2279	0·8596	0·5767	0·2370	0·8380	0·238 (4)
C(10)	0·6826	0·1359	0·9866	0·6860	0·1378	0·9750	0·119 (4)
C(11)	0·6894	−0·1398	0·9635	0·6860	−0·1378	0·9750	0·119 (4)
C(12)	0·5822	−0·2462	0·8164	0·5767	−0·2370	0·8380	0·235 (4)
N(1)	0·3737	−0·1917	0·5680	0·3686	−0·1659	0·5788	0·365 (4)
N(2)	0·3634	0·1401	0·5896	0·3686	0·1659	0·5788	0·365 (5)
N(3)	0·5399	0·3015	0·8323	0·5474	0·3127	0·8027	0·316 (4)
N(4)	0·7426	0·1317	1·0617	0·7458	0·1301	1·0498	0·117 (4)
N(5)	0·7491	−0·1286	1·0380	0·7458	−0·1301	1·0498	0·117 (4)
N(6)	0·5549	−0·3239	0·7731	0·5474	−0·3127	0·8027	0·316 (4)
N(1*c*)	0·8551	−0·0065	0·6206	0·8551	0	0·6206	0·085 (15)
C(1*c*)	0·8912	0·0288	0·4663	0·8912	0	0·4663	0·378 (18)
C(2*c*)	0·7966	0·0542	0·6118	0·8136	0·0823	0·6052	0·50 (3)
C(3*c*)	0·8305	−0·1103	0·5985	0·8136	−0·0823	0·6052	0·51 (2)
C(4*c*)	0·9042	0·0020	0·8090	0·9042	0	0·8090	0·03 (3)

the resulting puckered sheets of strongly interacting anions may be seen in the orthogonal views of Figs. 4 and 5. Fig. 4 represents a bounded projection, in which anion *A* corresponds to the coordinates listed in Table 1 with respect to the origin located at the intersection of [$\bar{1}$10] and [111]. As seen in Fig. 4, the plane of anion *B* is 0·32 Å further from the viewer than the plane of anion *A*. The plane of anion *C* is 0·79 Å nearer and that of anion *D* is 0·46 Å nearer the viewer. Anion *E* is 1·60 Å further from the viewer than the plane of anion *A*, with anions *F* and *G* respectively further away by 1·92 and 0·81 Å. Within the resulting puckered sheets such as those represented in Figs. 4 and 5, the sequence *ABCD*... forms a strand. The distance between adjacent strands *ABCD*... and *EFGH*... is greater than 4·8 Å. Within a strand, the shortest contacts are N(4)···N(4′) and N(5)···N(5′) of 3·189 (3) and 3·256 (3) Å, which make angles of 4·4 (1) and 0·4 (1)° respectively with the anion plane, and that pass through inversion centers. The next-nearest contacts are between pairs of anions within a column, as illustrated in Fig. 5. Such pairs are also related by inversion centers.

Overlap between radical anions forming a column is close, see Fig. 6: in phase II, the shortest distances between anion pairs are C(1)···C(4′) = 3·241 (2), C(2)···C(7′) = 3·288 (2), C(3)···C(8′) = 3·275 (2),

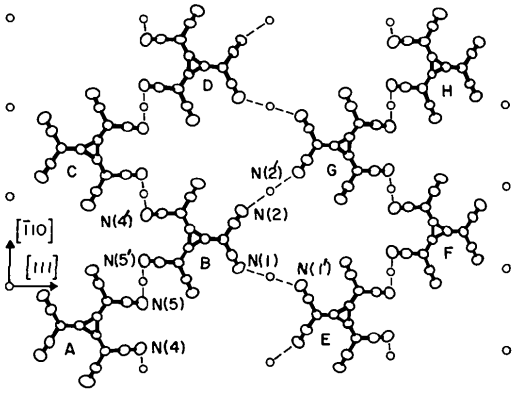

Fig. 4. Two partial strands of $HCTMCP^-$ radical anions with connecting short contacts N(5)···N(5′) = 3·256 Å from *A* to *B* and N(4)···N(4′) = 3·189 Å from *B* to *C*. Radicals in the *EFGH*... strand are separated by N(1)···N(1′) and N(2)···N(2′) distances, greater than 4·84 Å, from those in the *ABCD*... strand. Half the inversion centers in this bounded projection are shown.

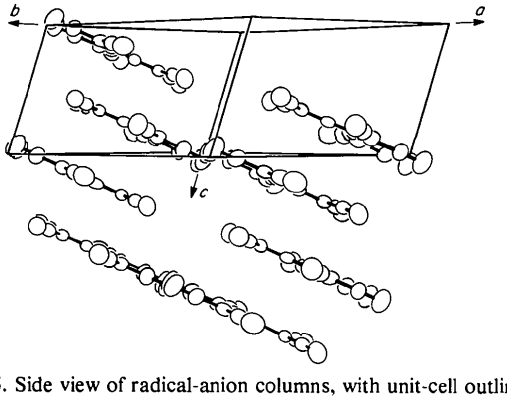

Fig. 5. Side view of radical-anion columns, with unit-cell outline, in phase II. The propagation direction of the columns is inclined at 11·8° to the *c* axis.

C(5)···N(1′) = 3·292 (2) and C(6)···N(2′) = 3·266 (2) Å. In addition, there are five identical contacts produced by the inversion center [C(4)··· C(1′) = 3·241 (2) Å *etc.*]. The strong interactions within strands and between pairs of closest anions in the columns result in quasi-two-dimensional magnetic order, since all strands are connected by the π-electron overlap, in contrast with phase I as discussed below. The interatomic distances connecting closest pairs of anions are normal, the shortest being 3·435 (2) Å for C(5)···C(7′).

In the case of $[(CH_3)_4N]^+$.HCTMCP$^-$, the magnetic exchange interaction J between spins along the strands through N···N contacts (*e.g.* on anions *ABCD*... in Fig. 4) clearly differs in strength from the interaction J' between closest pairs of anions in the columns due to π–π overlap in the direction normal to the anion plane, see Fig. 5. It is assumed that $J' < kT_c < J$ (k is the Boltzman constant), for a phase transition at T_c, since π–π overlap is greatly reduced in phase I. T_c is known to be 364 K: the increasing paramagnetism at 400 K is taken as indicative of a higher exchange interaction temperature that is on the order of 500 K (Abrahams *et al.*, 1984).

π-Electron bonding between HCTMCP$^-$ radicals in phase II

The combination of radical-anion molecular overlap illustrated in Fig. 6 and interatomic distances ranging from 3·24 to 3·29 Å between closest pairs of HCTMCP$^-$ anions in the columns is characteristic of π-electron-overlap bonding (*cf.* Soos, 1974; Herbstein, 1971). However, the present overlap does not lead to high electrical conductivity as found, for example, in TTF–TCNQ (*cf.* Alcácer, 1980) but is eight or more orders of magnitude lower (Abrahams *et al.*, 1984). The closest interatomic C···C or C···N approaches in TTF–TCNQ (Kistenmacher *et al.*, 1974) are 3·25 and 3·28 Å respectively, almost identical to the shortest

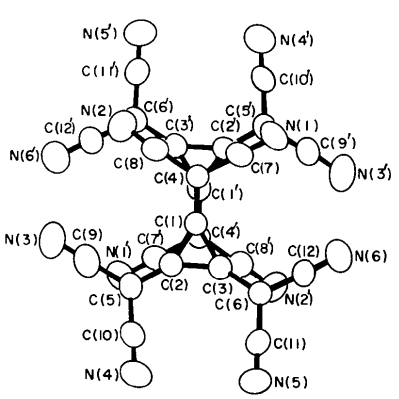

Fig. 6. Molecular overlap in phase II at 294 K between nearest pairs of HCTMCP$^-$ radicals normal to the anion plane.

Table 4. *Shortest intermolecular contacts* (Å) *between stacked anions in each of the two phases*

	294 K Phase II	388 K Phase I
C(1)···C(4′)	3·241 (2)	3·353 (6)
C(2)···C(7′)	3·288 (2)	*
C(3)···C(8′)	3·275 (2)	3·353 (4)
C(5)···N(1′)	3·292 (2)	3·360 (5)
C(6)···N(2′)	3·266 (2)	†

* Identical to C(3)···C(8′).
† Identical to C(5)···N(1′).

values in phase II of $(CH_3)_4N^+$.HCTMCP$^-$ (see Table 4). The shortest interplanar distance between stacks of TCNQ anions is 3·17 Å as compared to 3·24 Å between HCTMCP$^-$ anions at 294 K and 3·35 Å at 388 K. The corresponding shortest interplanar distance in TEA–$(TCNQ)_2$ is even less at 3·11 Å, as reported by Filhol & Thomas (1984). The high resistivity of the present material, in view of the contributing aromatic-like structures in Fig. 3 and the expected π–π overlap between radical anions, is presumed due to a delocalization energy smaller than that derived from contributions to the HCTMCP$^-$ radical such as are indicated in Fig. 3, resulting in all spins becoming largely localized.

The N(4)···N(4′) and N(5)···N(5′) contacts in phase II of 3·189 (3) and 3·256 (3) Å that are close to the plane of the HCTMCP$^-$ radical anion represent significant atomic interactions: the nitrogen van der Waals diameter in cyanogen (oxalonitrile), for example, is 3·54 Å (Parkes & Hughes, 1963) and N···N distances involving cyano groups are not often reported less than 3·4 Å (see, for example, Albertsson, Oskarsson & Ståhl, 1982). It may be noted that the present short N···N contacts make angles of 88·1 (1) and 83·1 (1)° respectively with the C(10)–N(4) and C(11)–N(5) bonds. These N···N interactions, characteristically oriented nearly normal to the adjacent C≡N bond and close to the cyclopropanide plane, are consistent with *p*-orbital overlap of the *sp*-hybridized N atoms.

Coulombic interactions between the radical anions and $[(CH_3)_4N]^+$ cations result in C(1*c*)···N(3) = 3·400 (8) and C(3*c*)···N(2) = 3·371 (7) Å as shortest contacts, where *c* represents a cation atom. All other cation–radical contacts are longer than 3·5 Å. Coulombic C···N interactions between NH_4^+ and CN^- of 3·04 Å are reported in NH_4CN (Lely & Bijvoet, 1944), and N···N interactions between NH_4^+ and $C(CN)_3^-$ of 2·93–3·17 Å in $NH_4C(CN)_3$ (Desiderato & Sass, 1965).

Quasi-one-dimensional radical anion array at 388 K and magnetic phase transition

The strong interactions within columns formed normal to the radical-anion plane at 294 K become much weaker at 388 K although molecular-overlap registra-

tion is even closer, as illustrated in Fig. 7. The anion orientation is similar in both phases, with the normal to the anion plane in phase I inclined at 9·0° to the *c* axis. Corresponding intermolecular distances in phase I for comparison with the phase II distances are given in Table 4. The average increase in length of about 0·08 Å for these C···C and C···N contacts in phase I results in intermolecular distances close to Pauling's (1960) van der Waals values. By contrast, the N(4)···N(4′) and N(5)···N(5′) interactions, which become identical at 3·234 (7) Å in phase I owing to the development of mirror symmetry in space group $C2/m$, are not significantly different from the mean value of the two room-temperature phase II distances, *i.e.* 3·223 Å. The temperature-independent interatomic interactions within the strands denoted by *ABCD... etc.* in Fig. 4 hence result in quasi-one-dimensional order above the phase transition. For recent reviews of the properties of low-dimensional ordered systems, see Alcácer (1980), Miller & Epstein (1978) and Keller (1975).

A quasi-two-dimensional magnetic spin array of uniform spacing, such as occurs in phase II, approaches an ideal two-dimensional Ising lattice (McCoy & Wu, 1973). The temperature dependence both of the lattice dimensions and the specific heat at the 364 K phase transition are consistent with a second-order phase transition (Abrahams *et al.*, 1984). As the transition is approached on heating, the increasing magnetic susceptibility appears due to enhanced antiferromagnetic ordering particularly between closest anion pairs within the columns of the quasi-two-dimensional array. It may be suggested that coupling between the lattice and this antiferromagnetic ordering leads to a lattice instability, resulting in the observed transition. The change in slope of the susceptibility–temperature dependence above the phase transition is fully consistent with a change from a quasi-two-dimensional array of antiferromagnetically coupled spins in phase II to a quasi-one-dimensional paramagnetic spin array in phase I.

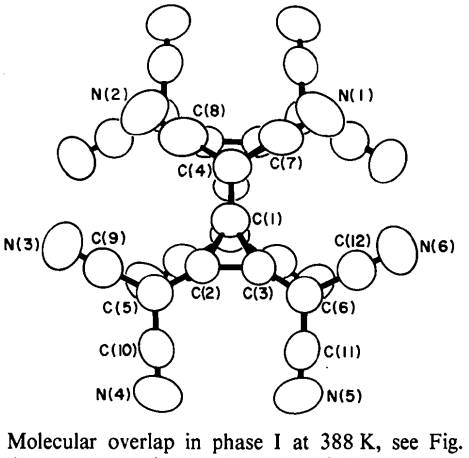

Fig. 7. Molecular overlap in phase I at 388 K, see Fig. 6, with mirror symmetry imposed by monoclinic space group.

The experimental results are hence in accord with a model in which exchange interactions J' between closest anion pairs in columns normal to the strands (see Fig. 5) are primarily antiferromagnetic and weaker than the antiferromagnetic interactions J along the strands. As J' tends to zero at 364 K, antiferromagnetic ordering associated with the columns breaks down and the spin array becomes increasingly paramagnetic as J/kT also decreases at higher temperatures.

Magnetic symmetry of phases I and II

Development of antiferromagnetic ordering in phase II is subject to the symmetry restrictions of the applicable Shubnikov group (see, for example, Koptsik, 1966). The point group for the magnetic structure may be taken as that of the crystal lattice, although corresponding unit-cell translations may be doubled. Experimental determination of such a possibility requires a neutron scattering study: however, only two Shubnikov groups may be derived from the space group of phase II that allows antiferromagnetism, namely $P\bar{1}'$ and $P_s\bar{1}$. The two remaining Shubnikov groups are $P\bar{1}$, which leads to a ferromagnetic array and $P\bar{1}1'$, which leads to either a paramagnetic or a diamagnetic array. The spins in $P\bar{1}'$ are reversed in sense across each anti-inversion center. Thus, in Fig. 2(*a*), a spin vector associated with one radical anion within the unit cell would be antiparallel to that of the other radical. In $P_s\bar{1}$, one unit-cell translation is doubled and inversion centers along that direction alternate with anti-inversion centers. Since spins related by anti-inversion centers are antiparallel and those by inversion are parallel, a zero net magnetic moment results in this space group. Loss of magnetic order associated with the columns in phase I, which are generally similar to those of phase II as shown in Fig. 5, and decreasing order in the strands of phase I giving rise to the paramagnetic contribution suggest that the magnetic symmetry above the phase transition corresponds to $C2/m1'$, the only 'grey' Shubnikov-group member of the $C2/m$ family.

It is a pleasure to thank Professor J. Albertsson for several calculations including evaluation of the displacements given in Table 3.

References

ABRAHAMS, S. C., BAIR, H. E., DISALVO, F. J., MARSH, P. & DEURING, L. A. (1984). *Phys. Rev. B*, **29**, 1258–1262.

ABRAHAMS, S. C., BERNSTEIN, J. L. & KEVE, E. T. (1971). *J. Appl. Cryst.* **4**, 284–290.

ABRAHAMS, S. C. & KEVE, E. T. (1971). *Acta Cryst.* A**27**, 157–165.

ABRAHAMS, S. C. & MARSH, P. (1987). *Acta Cryst.* A**43**, 265–269.

ALBERTSSON, J., OSKARSSON, Å. & STÅHL, K. (1982). *Acta Chem. Scand. Ser. A*, **36**, 783–795.

ALCÁCER, L. (1980). Editor. *The Physics and Chemistry of Low-Dimensional Solids*. Dordrecht: D. Riedel.

ALLEN, F. H. (1980). *Acta Cryst.* B**36**, 81–96.
AMMON, H. L., SHERRER, C. & AGRANAT, I. (1977). *Chem. Scr.* **11**, 39–43.
BECKER, P. J. & COPPENS, P. (1975). *Acta Cryst.* A**31**, 417–425.
BUSING, W. R., MARTIN, K. O. & LEVY, H. A. (1973). *J. Appl. Cryst.* **6**, 309–346.
DESIDERATO, R. & SASS, R. L. (1965). *Acta Cryst.* **18**, 1–4.
DIETRICH, H. (1970). *Acta Cryst.* B**26**, 44–55.
Enraf–Nonius (1982). *Enraf–Nonius CAD-4 Operation Manual.* Enraf–Nonius, Delft.
FILHOL, A. & THOMAS, M. (1984). *Acta Cryst.* B**40**, 44–59.
HERBSTEIN, F. H. (1971). *Perspectives in Structural Chemistry* IV, edited by J. D. DUNITZ & J. A. IBERS, pp. 166–395. New York: Wiley.
International Tables for X-ray Crystallography (1974). Vol. IV. Birmingham: Kynoch Press. (Present distributor D. Reidel, Dordrecht.)
JAUD, J., CHASSEAU, D., GAULTIER, J. & HAUW, C. (1974). *C. R. Acad. Sci.* **278**, 769–771.
JOHNSON, C. K. (1976). *ORTEP*II. Report ORNL-5138. Oak Ridge National Laboratory, Tennessee, USA.
KELLER, H. J. (1975). Editor. *Low-Dimensional Cooperative Phenomena.* New York: Plenum.
KISTENMACHER, T. J., PHILLIPS, T. E. & COWAN, D. O. (1974). *Acta Cryst.* B**30**, 763–768.
KOPTSIK, V. A. (1966). *Shubnikov Groups.* Moscow State Univ. Press.
LELY, J. A. & BIJVOET, J. M. (1944). *Recl Trav. Chim. Pays-Bas*, **63**, 39–43.
LISSALDE, F., ABRAHAMS, S. C. & BERNSTEIN, J. L. (1978). *J. Appl. Cryst.* **11**, 31–34.
LUNDGREN, J.-O. (1982). Crystallographic computer program. Report No. UUIC-BB-4-05. Univ. of Uppsala, Sweden.
MCCOY, B. M. & WU, T. T. (1973). *The Two-Dimensional Ising Model.* Harvard Univ. Press.
MAIN, P., HULL, S. E., LESSINGER, L., GERMAIN, G., DECLERCQ, J.-P. & WOOLFSON, M. M. (1978). *MULTAN*78. *A System of Computer Programs for the Automatic Solution of Crystal Structures from X-ray Diffraction Data.* Univs. of York, England, and Louvain, Belgium.
MILLER, J. S. & EPSTEIN, A. J. (1978). Editors. *Synthesis and Properties of Low-Dimensional Materials.* New York Academy of Sciences.
MORTENSEN, M. (1982). *Phys. Scr.* **25**, 854–856.
PARKES, A. S. & HUGHES, R. E. (1963). *Acta Cryst.* **16**, 734–736.
PAULING, L. (1960). *The Nature of the Chemical Bond,* 3rd ed. Ithaca: Cornell Univ. Press.
POUGET, J. P., SHIRANE, G., BECHGAARD, K. & FABRE, J. M. (1983). *Phys. Rev. B*, **27**, 5203–5206.
RINDORF, G., SOLING, H. & THORUP, N. (1982). *Acta Cryst.* B**38**, 2805–2808.
SOOS, Z. G. (1974). *Annu. Rev. Phys. Chem.* **25**, 121–153.
SUNDARALINGAM, M. & JENSEN, L. H. (1966). *J. Am. Chem. Soc.* **88**, 198–204.
SUTTON, L. E. (1965). *Tables of Interatomic Distances and Configuration in Molecules and Ions. Supplement.* Spec. Publ. No. 18. London: The Chemical Society.
WARD, M. D. (1987). *Organometallics*, **6**, 754–762.

Acta Cryst. (1988). B**44**, 271–281

Thermal Vibrations and Electrostatic Properties of Parabanic Acid at 123 and 298 K

BY X. M. HE,* S. SWAMINATHAN AND B. M. CRAVEN†

Department of Crystallography, University of Pittsburgh, Pittsburgh, PA 15260, *USA*

AND R. K. MCMULLAN

Chemistry Department, Brookhaven National Laboratory, Upton, NY 11973, *USA*

(*Received* 8 *June* 1987; *accepted* 4 *November* 1987)

Abstract

The crystal structure of parabanic acid (1*H*,3*H*-imidazoletrione, $C_3H_2N_2O_3$, $M_r = 114{\cdot}1$) at 123 K [monoclinic, $P2_1/n$, $Z = 4$, $a = 10{\cdot}704\ (2)$, $b = 8{\cdot}187\ (2)$, $c = 4{\cdot}969\ (1)$ Å, $\beta = 92{\cdot}32\ (1)°$] has been determined by neutron and X-ray diffraction. Neutron reflections [1658, $(\sin\theta)/\lambda \leq 0{\cdot}78$ Å^{-1}, $\lambda = 1{\cdot}0470\ (1)$ Å, $\mu = 0{\cdot}75$ cm^{-1}] in full-matrix least-squares refinement ($wR = 0{\cdot}055$) gave nuclear parameters with bond lengths having estimated standard deviations (e.s.d.'s) of 0·001 Å. X-ray reflections [3150 with $|F| \geq 3\sigma$ and $(\sin\theta)/\lambda \leq 1{\cdot}3$ Å^{-1}, Mo $K\alpha$, $\lambda = 0{\cdot}7093\ (1)$ Å, $\mu = 1{\cdot}708$ cm^{-1}] were used in full-matrix least-squares refinement ($R = 0{\cdot}022$) assuming Stewart's rigid pseudoatom model, so as to determine the charge-density distribution. Sharp features near the O nuclei in the residual electron density map noted by Craven & McMullan (CM) [*Acta Cryst.* (1979), B**35**, 934–945] in their 298 K study were absent at 123 K. New refinements using CM's 298 K data give significant third-order thermal parameters for O atoms due to anharmonic molecular stretching, with good agreement between probability density functions, (p.d.f.'s) from X-ray and neutron diffraction. When deconvoluted from the thermal vibrations in the crystal, deformation charge densities derived at 298 and 123 K are in satisfactory agreement and conform closely to the 2*mm* symmetry of the isolated molecule. The molecular dipole moment is 2·3 (3) D [7·7 (10) × 10^{-30} C m]. A map of molecular electrostatic potential indicates that

* Present address: Department of Biology, University of Utah, Salt Lake City, UT 84112, USA.
† To whom correspondence should be addressed.

0108-7681/88/030271-11$03.00 © 1988 International Union of Crystallography